Astrometric Demonstrator in Optical Interferometry with the test siderostats at Paranal

G. Daigne[a], F. Delplancke[b], F. Arenou[c], F. Derie[b], P. Dierich[c], M. Odenkirchen[d], J. Palasi[c] and A. Glindemann[b]

[a]Observatoire de Bordeaux, BP-89, 2 rue de l'Observatoire, F-33270 Floirac, France
[b]ESO, Karl-Schwarschildstr. 2, D-85748, Garching b. München, Germany
[c]Observatoire de Paris-Meudon, 5 Place J. Janssen, F-92195 Meudon, France
[d]Sternwarte der Universität Bonn, Auf dem Hügel 71, D-53121 Bonn, Germany

ABSTRACT

We propose a near-IR demonstration experiment with the two VLTI test siderostats (0.4 m) at Paranal, to be used both in wide-angle single-field and in narrow-angle dual-field astrometry. The specifications required to operate an astrometric interferometer are particularly stringent on siderostat rotation axes, pupil transfer and instrument stability. These problems, together with the instrument capabilities in the two operation modes, are detailed in this paper. The present time accuracy of reference stars is evaluated, as well as statistical properties of the dual-field targets. The astrometric testbed instrument will be of great help in analyzing and understanding, on site, the main features of the VLTI, in order to optimize its future operation with Auxilliary Telescopes in phase referenced imaging and astrometric modes (PRIMA).

Keywords: Optical interferometry, Astrometry, Stellar reference frame, Binary stars

1. INTRODUCTION

A few optical interferometers are going to be equipped with dual-field facilities, the Palomar Testbed Interferometer[1,2] (PTI) being *the* prototype of such an instrumentation. With simultaneous observation of two sources at a very-small angular distance, a dramatic reduction of the effects of atmospheric fluctuations has been shown[3] and a repeatability of 0.1 milliarcsec (mas) in narrow-angle measurements is obtained with PTI. The goal of dedicated dual-field instrumentation (Keck Interferometer and its outriggers, Very Large Telescope Interferometer[4–6] and its Auxiliary Telescopes) is an astrometric uncertainty of 10-20 μas, the angular distance between the two sources being about the size of the isoplanatic angle, or less than 20" in the K band.

Scientific objectives of dual-field interferometry have been advocated elsewhere (cf. Ref. 7), detection and mass determination of sub-stellar companions being one of the main objectives. Following preliminary studies,[8] and in advance of dual-field astrometry with the Auxiliary Telescopes (ATs), we propose a prototype experiment with the VLTI test siderostats at Paranal.[9] We argue that first interferometric equipments (test siderostats, main delay lines, beam handling ...) should be adequate for performance demonstration in wide-angle astrometry and hence, with some additional care, in narrow-angle astrometry.

Baseline calibration of the interferometer relies on single-field observation of reference stars. As underlined by several authors (cf. Ref. 10), relative baseline uncertainty has to be smaller than the expected relative uncertainty on narrow-angle measurements, that is smaller than one part per million, which is a (much) weaker constraint than for 'global' astrometry. If we consider the geometry of baseline calibration with the test siderostats at Paranal (Sect. 3.2), the relative uncertainty on baseline vector should be as small as 10^{-7}, or 20 mas in baseline orientation. This is about the accuracy already achieved in wide-angle astrometry with the USNO Mark III interferometer,[11–14] the stellar reference frame being then the FK5 with its zonal errors and astrometric uncertainty.[15]

With the Hipparcos stellar frame and the FK6, with accurately known station coordinates and Earth rotation parameters, the situation has improved for wide-angle optical astrometry as compared to the 1980's. Furthermore,

Send correspondence to G. Daigne or F. Delplancke
E-mail: daigne@observ.u-bordeaux.fr, or fdelplan@eso.org

estimated accuracy of the Hipparcos frame for the 2000's is proceeding in a range now accessible to ground-based optical interferometry, which makes a challenge.

Another topic to be documented with the proposed experiment is *piston and differential piston fluctuations*. Ground-based optical astrometry needs averaging atmospheric fluctuations on long durations. In a sense, it is a time-consuming technique. Getting a first experience with siderostats will help quantify the performances achievable with larger apertures. Do we recover the outer scale of turbulence as measured with a dedicated instrumentation[16]? What is the validity of the frozen-in or Taylor hypotheses in altitude? Is there any difference between "isoplanatic angle" and "isopistonic angle"[17] ?

The two operation modes, wide-angle and narrow-angle astrometry, are respectively described in Sect. 2 and Sect. 3 , together with stability requirements and statistical data on reference stars and binary targets. The proposed implementation at Paranal is further developed in Sect. 4.

2. WIDE-ANGLE ASTROMETRY

2.1. Basic relation

With zeroing atmospheric piston and residual phase delay, a simplified equation for wide-angle or single-field astrometry is:

$$\vec{B} \cdot \vec{S} - L_{\rm del} + C_{\rm off} \simeq 0, \qquad (1)$$

where $\vec{B}$ is the baseline vector and $\vec{S}$ a unit vector in the source direction outside the atmosphere, supposed to be plane stratified above the interferometer (not too long a baseline). The scalar product $\vec{B} \cdot \vec{S}$ is known as the geometric Optical Path Delay, $OPD_{\rm geo}$, which is wavelength independent. The source direction is supposed to be known, in a topocentric frame, together with its time variations (Earth rotation). In a real world, time variations of the geometrical OPD will not be given only by Earth rotation; baseline variations will have to be considered and modeled.

The second term in the previous equation is the interferometer delay; its variations with source tracking are measured by the main delay line metrology system. With non-evacuated delay lines, the metrology data will be converted to the effective or leading wavenumber of group delay tracking,[18,19] with a few 10^{-8} as relative uncertainty. Such a value is quite consistent with the planned 1 μm accuracy in along track positioning of the delay lines.[6]

The interferometer 'constant' or offset $C_{\rm off}$ is the arms imbalance which cannot be determined by the main delay metrology. As there is no mean to get rid of this quantity, the interferometer design should minimize its time variations and maximize its reliability. This is further developed in Sect. 2.3.

2.2. Baseline variations

Baseline variations hold for variations left in the scalar product $\vec{B} \cdot \vec{S}$ once Earth rotation has been modeled. The Earth rotation parameters are accurately known from VLBI observations and GPS measurements. The geocentric coordinates of the interferometer are supposed to be measured also by GPS (≤ 0.1 m uncertainty). The contributions left are at least of 4 kinds:

- local deformations of the terrestrial crust, either tideal or seismic,
- displacements of the siderostat mounts due to thermal effects,
- axis-misalignments of the siderostat mounts,
- vibrations of the siderostats during source tracking.

The longitudinal scale of short term crust motion is much larger than the interferometer baseline. The effect on baseline variations can be represented with two angles, in a way similar to 'vertical deviation'. Among the sources of platform variations, terrestrial tides have a peculiar signature and might be detected if their amplitude is larger than a few 10 mas.

Baseline variations due to thermal effects on the siderostat mounts have been a main concern with the Mark III interferometer.[11] With the VLTI test siderostats, the main part of the mount stands underground and thermal effects should be better controlled.

If the two rotation axis of the siderostats do not intersect exactly, the instantaneous pivot point is no longer fixed in a local frame. Furthermore, with axis offsets slightly different from one to the other siderostat, the baseline vector is changing with source direction. The first harmonic of such axis-misalignments has been modeled for the ATs, with 3 parameters,[20] and a similar model will be fitted to siderostat tracking.

Driving motors and gears might be a source of vibrations, although the test siderostats at Paranal show up particularly smooth. Wind varying pressure on the tiltable flat is expected not to add piston noise nor to reduce visibility measurements. On the contrary, laser monitoring of the tiltable flats would be needed.

2.3. The interferometer constant

One of the most critical part in long-baseline interferometry is pupil transfer, from the telescope/siderostat input to the combination plane. Indeed, the optical system from siderostat input to beam combination has to be both active, for source tracking, and adaptive, for tip/tilt and piston corrections. Optical path variations induced by beam misalignment could be a problem if the position of the light beam, between siderostat input and tip/tilt correction mirror in the interferometric laboratory, is not carefully controlled.

The proposed setup relies on pupil imaging by the cat's eye of the main delay line and its Variable Curvature Mirror (VCM).[21] The beam along the interferometer arm will have its entrance pupil reimaged onto the tiltable flat of the field selector in the lab. To first order, the optical path between the two conjugated planes is not dependent on their relative tilt (stigmatism). Furthermore, light beam directions will be locally controlled at the two ends of the interferometer arm. The longitudinal positioning of the pupil will be also adjusted with the help of the dual-field separator and its differential metrology system (Sect.4).

While stiffening pupil transfer along the interferometer arm, a more reliable interferometer constant is expected. This should be demonstrated with wide-angle astrometric observations.

2.4. Reference stars

The accuracy of the positions of reference stars at epoch 2003.0 has been analysed. The most accurate astrometric data for bright sources (i.e. not quasars) are provided by the Hipparcos catalogue[22] and by the new FK6.[23] Due to the short time span of the Hipparcos mission (3 years), the observed proper motion may not represent the true long-term mean motion of a star, but merely the tangential signature of a more complex apparent displacement. In principle, the only way to obtain a reliable prediction of future reference positions is to choose stars with linear motion, apart from the parallactic wobble, or systems with well-known orbits. The latter is of course very rare. To minimize the risk of contamination by orbital motion, we omit all Hipparcos stars classified as G-, X- or V-solutions, as well as suspected binaries (flagged S) and known double or multiple systems (classified as C), except for wide pairs observed by two different pointings. In the case of the FK6 we do not apply special selection criteria. However we note that there is an option to restrict the FK6 to the 50% subsample of astrometrically excellent stars, *i.e.* those without any significant deviation in the comparison of short-term and long-term proper motion.

Table 1. Median value of position errors of reference stars at epoch 2003.0, in declination zone [$-10°$, $-70°$]. N is the number of stars found with different sensitivity threshold.

	K_{lim} mag	N	$\sigma_\alpha \cos\delta$ mas	σ_δ mas
Hipparcos	5.0	6404	8.9	7.7
	7.0	18626	9.7	8.4
	9.0	35370	10.7	9.3
FK6	7.0	323	4.7	4.4

The instrumental selection criteria are:

- sky coverage, within a declination zone [$-10°$, $-70°$],
- magnitude limit in the visible $V \leq 9.0$, for siderostat tracking ,

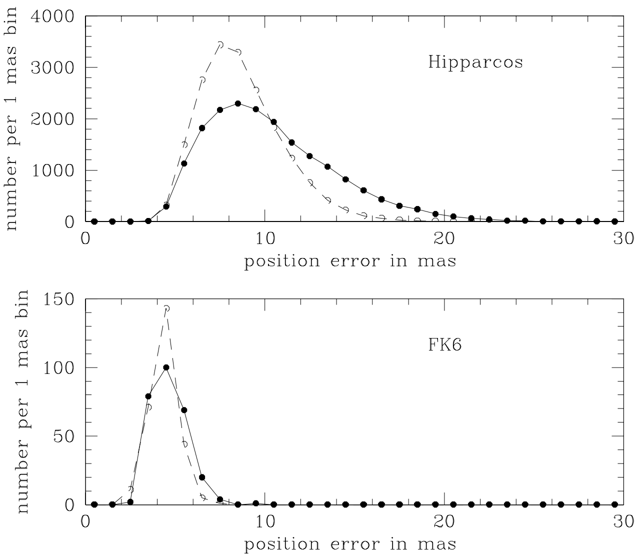

Figure 1. Distribution of position errors for Hipparcos and FK6 stars with $K \leq 7.0$ at epoch 2003.0, in declination zone $[-10°, -70°]$. Solid line: right ascension ($\sigma_\alpha \cos\delta$), dashed line: declination (σ_δ).

- magnitude limit in the K band given by the interferometer sensitivity threshold $K = 7.0$.

The K-magnitude of the stars was estimated from the V and $(B - V)$ given in the Hipparcos catalogue, and the approximation $K \simeq V - 2.4 \cdot (B - V)$ which is a linear fit to a more elaborate model,[24] valid for spectral types F0 to K5 (giants and dwarfs) and for metal-rich stars. The relation will give an underestimate of the K-magnitude for metal-poor stars, and for M dwarves.

The errors of the individual positions at epoch 2003.0 have been derived from the catalogue errors in position, proper motion and parallax and their correlation (in case of Hipparcos). The median position errors are given in Table 1 for the Hipparcos and FK6 catalogues, together with the number of stars for different K-magnitude limits. The histogram of position errors is plotted on Fig. 1 for $K \leq 7.0$. The FK6 prediction at 2003 would be about twice as much accurate as the Hipparcos one. Typical errors are 5 mas, and the error distributions are narrower than with Hipparcos, particularly in right ascension (mainly due to the scanning law of the satellite in this limited sky area).

2.5. Observing sequence

A wide-angle observing sequence is made of sequential observations of stars scattered in the siderostat field of view (FOV): a half cone angle of at least 30 degrees centered at a zenithal distance of 15 degrees South (Sect. 4.1). Alltogether 7 parameters are to be estimated with the observation of reference stars: baseline orientation and length, interferometer constant, and siderostat tracking model (3 parameters). We may expect the siderostat model to be checked once in a while if reliable, so that we are left with 4 parameters. The distribution and number of reference stars together with sequence duration will be optimized. With observing sequences of one hour duration, and 5 minutes per single observation, a duty cycle of about 50% could be reached, half of the time being spent for calibration.

Most of the FK6 stars do have a K-magnitude smaller than 5. Their density will be about 2 per 100 square degrees, or about 56 stars in the siderostat FOV. It makes plenty of objects for baseline calibration.

3. NARROW-ANGLE ASTROMETRY

3.1. Basic relation

We may start with two relations similar to Equ. 1, with indices $i = 1, 2$ for each one of the sources simultaneously observed:

$$\vec{B}_i \cdot \vec{S}_i \; - \; L_{i,\mathrm{del}} \; + \; C_{i,\mathrm{off}} \; \simeq \; 0. \tag{2}$$

Once again, atmospheric (differential) piston is averaged to zero in this analysis, mainly focused onto the optical system of the interferometer. A first question is to know which ones of the 3 interferometer related quantities do take the same value, or how much do they differ from one source to the other.

Baseline difference at a precision level of a few nanometer cannot be estimated through wide-angle astrometric calibration. The baseline vector has to be the same for the two source directions due to the interferometer design itself. Among the 4 kinds of baseline variations (Sect. 2.2), misalignments and vibrations could induce some baseline differences. A way to minimize their effects is to have, as much as possible, the same pupil-prints on the tiltable flat of the siderostat for the two observed field directions. The pupil-print is here the backward image, along the interferometer arm, beam compressor and fixed siderostat flat, of the pupil realized in the lab, at the combination/ detection level. With a common baseline, the basic relation for differential astrometry will be:

$$\vec{B} \cdot (\vec{S_2} - \vec{S_1}) \; - \; \Delta L_{\rm del} \; + \; \Delta C_{\rm off} \; \simeq \; 0, \tag{3}$$

where the first term is the differential OPD to be measured.

3.2. Baseline calibration, what is required for narrow-angle astrometry?

The angular distance $\Delta\vec{S} = \vec{S_2} - \vec{S_1}$ is so small that, for error estimate, differential OPD can be replaced by the product $\vec{b} \cdot \Delta\vec{S}$ where $\vec{b}$ is the baseline projection on the celestial sphere. The projected angle to be measured is $\Delta S = \Delta\vec{S} \cdot \vec{b}/b$. In terms of baseline uncertainty, the angle uncertainty will be:

$$\delta(\Delta S) \; = \; \Delta\vec{S} \cdot \delta\vec{b}/b, \tag{4}$$

where $\delta\vec{b}/b$ is the relative uncertainty on the baseline vector perpendicular to the line of sight.

On the contrary, only the baseline component along the line of sight is measured in wide-angle or single-field astrometry (Equ. 1), and observations in different directions are needed for baseline calibration. Suppose the observed directions are regularly distributed in a circular field of view with radius Θ, the average angular distance to the field center will be $\Theta_m \simeq 2\Theta/3$. If α is the relative uncertainty on baseline calibration along the field center, the relative uncertainty in a perpendicular direction will be $\beta = \alpha/\tan(\Theta_m)$, that is $\beta \simeq 2.7\alpha$ with $\Theta = 30$ degrees.

Considering that baseline calibration is only one among the several error sources in dual-field astrometry, we demand that the variance of each identified error source should not exceed a tenth of the total allowed variance. One part per million for the (total) uncertainty in dual-field astrometry will require $\beta \leq 3 \cdot 10^{-7}$, that is a relative uncertainty $\alpha \simeq 10^{-7}$, or 20 mas, in wide-angle astrometry. A 50 m baseline will translate it into 5 μm uncertainty in the source direction. On the perpendicular direction (mainly horizontal plane), the baseline uncertainty could reach 14 μm. Such a ratio of about 3 has been previously found in a simulation of baseline calibration for the ATs.[20]

3.3. Differential quantities

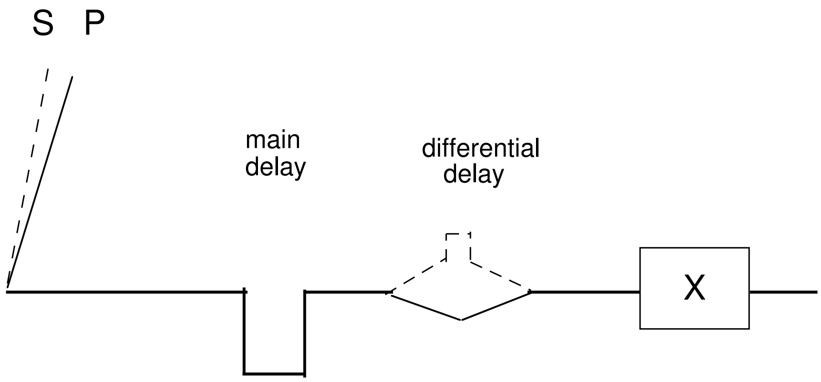

Figure 2. Dual-field interferometry for simultaneous observation of a primary (P) and a secondary (S) source with a common main delay line, and differential delay in one of the light path. A single arm of the interferometer is shown.

For symmetry reasons, the two interferometer arms should be as much as possible identical, except for the positions of their delay lines. A single arm is shown on Fig. 2. Delay variations and interferometer offsets can be related to a single arm if the other is taken as reference.

The differential delay ΔL_{del} in Equ. 3 is the sum of two contributions:

$$\Delta L_{\mathrm{del}} = \Delta\epsilon_* L_{\mathrm{del}} + \Delta l, \qquad (5)$$

the first one being a correction for longitudinal dispersion with two stars and different light spectra in the near-IR. With group delay tracking, $\Delta\epsilon_*$ can reach a few 10^{-9} for cool stars and different spectral types.[19] The second term compensate for differential OPD between the two sources, that is almost 0.01 m for 50 m baseline. Corrections for longitudinal dispersion at a precision level of a few nm will be rather straightforward, and differential metrology can be performed in the visible range.

The remaining term in Equ. 3 is the differential "constant" or offset between the two light paths along the interferometer arms. We emphasize that it cannot be measured through metrology, nor its time variations monitored with the required precision level. The main problem may not be the metrology itself, but the unavoidable differences between the paths of star light and metrology (beam size, wavelength, optical components, ...). The differential "constant" could be calibrated, and its variations monitored, with timely observations of an astrometric reference pair. The drawback of such a procedure is that significant changes in siderostat pointing and main delay line position will be needed. Another way is to have an observing sequence with interchanges of the relation between source (Primary/Secondary) and beam number (1/2) in the interferometer arm, and in the combination unit. An observing sequence will be made of 4 phases, and its total duration will be short enough for the differential "constant" to be considered as not varying. It is further described in a forthcoming paper on the control of an optical interferometer arm.

3.4. Dual-field targets

In the dual-field astrometric mode considered in this paper, the "target" and "reference" stars are supposed to be bright enough for fringe tracking, that is both with $K \leq 7.0$ as in Sect.2.4. Due to the low density of bright stars, the probability of observing by chance two stars with an angular separation smaller than 30" will be very low, and most of the candidate visual pairs will be long-period binaries. We investigate their distribution in the declination range $[-10°, -70°]$.

The Hipparcos catalogue[22] is *the* starting data base for such an investigation:

- the Hipparcos Input Catalogue[25] has been built from scientific proposals. It includes the Gliese Catalogue of nearby stars, as well as catalogues of stars with large proper motion. All these objects were given high priority, so that the Hipparcos catalogue is reasonably complete within 20 parsecs, up to $V \leq 10.5$.
- Due to the Hipparcos observing constraints, the duplicity had to be checked in advance, from ground-based observations compiled into the CCDM Catalogue.[26] Pairs with a large magnitude difference may not have been accounted for, in which case they also are not suited targets for dual-field observations of bright pairs.

We found 89 pairs of *K-bright* stars with angular separation 3" $\leq \rho \leq$ 30", $V \leq 9$ for at least one of them, and a relative parallax uncertainty smaller than 20%. About 50 pairs are within 50 pc, and 20 within 25 pc. The distribution of approximate K-magnitude difference is shown in terms of the angular separation on Fig. 3a. The lack of pairs with large magnitude difference may be due to selection effects.

For a given mass ratio between a star and its low-mass companion, the reflex motion of the parent star increases as the 2/3 power of the orbital period, and is proportional to the parallax. A ten Jupiter-mass planet orbiting around a solar-like star with a period of 4 years at a distance of 80 pc induce a 0.3 mas astrometric amplitude. With 0.1 mas for the mean precision on each relative positions, it should be detected with a good confidence level. The 0.3 mas detection threshold has been used in the following estimate of the detection rate in terms of companion mass, for different orbital periods.

Star masses have been estimated from their absolute magnitude, with the help of the Henry & McCarthy[27] relation, assuming the same parallax for both components of each pair. A dark companion with a given mass can be detected or not depending on the orbital period and star distance. Summing over all stars in the sample, we

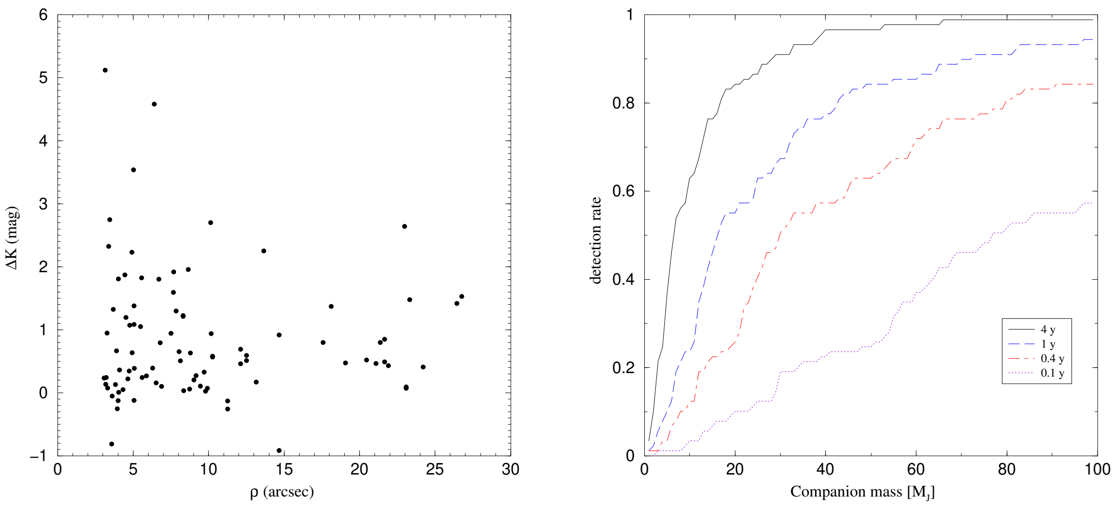

Figure 3. Data on selected *K-bright* binaries in the Hipparcos catalogue, in the declination range [−10°, −70°]. (a) K-magnitude difference in terms of the angular separation, in the range [3",30"]. (b) Estimate of the detection rate of dark companions in terms of their mass (Jupiter mass), for different orbital periods: 4 years (solid line), 1 year (dashed line), 0.4 year (dot-dashed line), and 0.1 year (dotted line). The detection threshold is 0.3 mas.

can estimate the mean probability to detect a companion with a given mass. This gives an upper estimate of the fraction of low-mass companions which can be detected in the sample (Fig. 3b). To convert it into an actual number of detection, it must be multiplied by the true frequency of low-mass companions orbiting one of the components in a binary system, which is still unknown. Assuming a 4% frequency as for the "Jupiter-like" planets found from spectroscopic studies,[28] and postulating no brown dwarf desert[29] for long periods, then a few detections would be obtained. Confirmation of companions already found by radial velocity studies will be obtained more easily, with a lower threshold for the astrometric signature.

The data reduction will have to take into account several astrometric effects, even with true binaries. As an example, a pair of solar-type stars separated by 20" at a distance of 20 pc will show a relative motion reaching about 20 mas/y, and second-order terms may be significant for nearby pairs at the 0.1 mas level.

4. IMPLEMENTATION AT PARANAL

The principle scheme of the astrometric demonstrator is given in Fig. 4. It will use most of the existing elements of the VLTI (siderostats, delay lines, beam compressors, and tip-tilt sensors) and most of the sub-systems which will be developed by ESO for PRIMA, the Phase-Referenced Imaging and Micro-arcsecond Astrometry facility (differential delay lines, fringe sensor units, and possibly the metrology). The demonstrator star separator will use the advantage of the large VLTI field of view (40") with the siderostats. The implementation of the demonstrator in Paranal will imply a very slight mechanical modification and an addition of optics on the siderostats, and a simple implementation of optical parts (beam splitters and mirrors) on the laboratory beam switchyard and on the PRIMA table. The modifications and the use of the current VLTI elements are detailed here below.

4.1. Test siderostats

The VLT test siderostats have a 400 mm mobile mirror on a stiff Alt-Az mount. They can point at zenital angles going from 60° North to 75° South, and at azimutal angles going from 60° East to 60° West.[9] A small portion of the pupil is vignetted by the siderostat mechanical part, in the meridian at zenital angles larger than 40°. The pupil is elongated in shape and varies in area with the pointing direction. The effective collecting aperture is on average 70 % of the maximum mirror collecting area, that is 0.088 m^2.

The siderostat optical principle scheme is given in Fig. 5. Mirrors M1, M2 and M5 are flat. M3 and M4 are confocal parabolas, respectively concave and convex, with a compression factor of 5. The output beam shape mimics

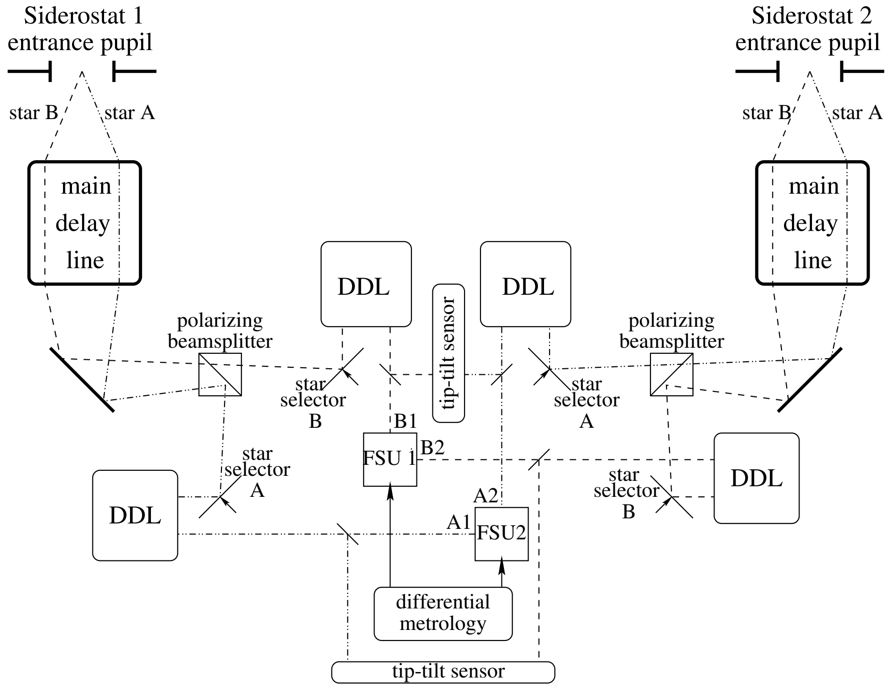

Figure 4. Principle scheme of the astrometric demonstrator in dual-field interferometry. The two stars are positioned symmetrically with respect to the optical axis of the siderostat/telescope and interferometer arm. In single-field, the two paths are aligned with the optical axis, and a single FSU can be used.

the input shape with a maximum diameter of 80 mm. All mirrors are Hard Gold coated and present an optical quality better than 25 nm RMS. The siderostats are equipped with visible tracking cameras using the photons of the central obscuration.

To implement the demonstrator, a metrology fringe detector will have to be introduced as close to M1 mirror as possible but without degrading the siderostat throughput and while still collecting photons. The only practical position is then on mirror M4, in the central obscuration (diameter 20 mm), as shown in Fig. 5. The CCD camera for differential metrology will be fixed on the siderostat mechanical structure, and a relay lens will imaged M4 on the camera through a hole drilled in the siderostat housing. These modifications are minor and could be made very stiff.

4.2. Relay optics, delay lines, cat's eye and VCM

The demonstrator will use exactly the same relay optics and delay lines as the usual VLTI single-field operation. Only one feed of the delay lines will be used, its field being 200", so 40" on the sky (compression factor of the siderostats = 5). We will limit the demonstrator to angles of 30" between both stars in dual field. The relay optics and delay line specifications are completely compatible with the demonstrator requirements.

The Variable Curvature Mirror (VCM) will transfer the siderostat pupil toward the interferometric laboratory. At the same time, it will transfer the metrology pupil from the laboratory toward the 45° mirror in the siderostat. At this condition, the two off-axis metrology beams (see Sect. 4.6) will interfere and fringes will be observed on the camera at the siderostat level. This property will be used to test the performances and the operation of the VCM.

The demonstrator will use only one special feature of the delay lines compared to the usual single-field VLTI operation : the 200" delay line field of view. It means that the two stars, in the dual-field mode will be imaged on 2 different points on the VCM, distant by at most 2.7 mm. The VCM achieved optical quality ($\lambda/6.5$ up to $\lambda/2.5$ PTV on a 5 mm diameter circle) is consistent with the demonstrator requirements. Furthermore, the demonstrator will be a useful tool to check the VCM optical quality once in operation. It is best when the curvature is low (mirror almost flat). Thus it will be better to work with the siderostats at locations where the entrance and output pupils

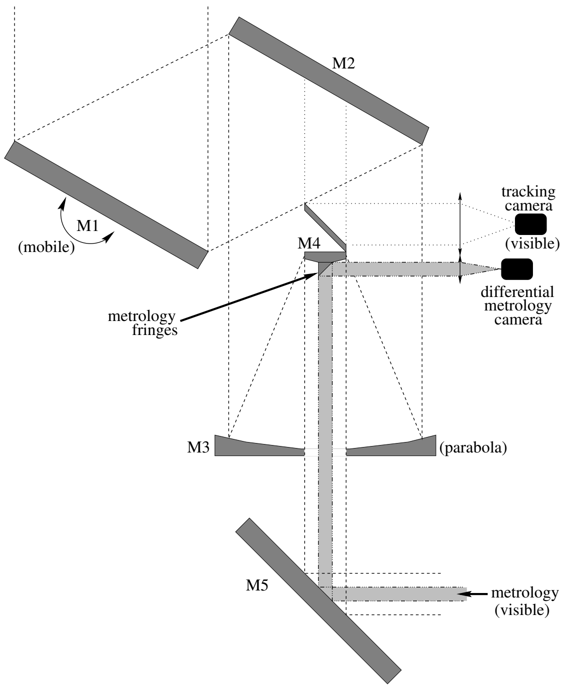

Figure 5. Principle scheme of the siderostats and of the implementation of the fringe sensing optics and camera for the differential metrology.

along the interferometer arm are not too far away, with nearly equal distances on either side of the delay line. The VLTI stations close to the interferometric laboratory are so preferred.

4.3. Star separator and tip-tilt sensors

Due to the large field of view of the delay lines when used with the siderostats, the star separator can be placed in the interferometric laboratory. A pupil amplitude beam division will be implemented, using a polarizing beamsplitter. A silica beamsplitter can reach a rejection factor of 10^2, which is enough for our purposes. With this solution, 50 % of the light will be lost but calibration is supposed to be eased and more accurate than with image plane star separation. The stars will then be selected and followed throughout the observation by means of two tip-tilt mirrors, in each interferometric arm. The mirrors will use feed-back signals coming from tip-tilt sensors to maintain the stars centered on the beam combiners (see Fig. 4). The selected light beams will then be sent to 4 differential delay lines (DDL), only one being active. From the DDL output beams, the J-band light will be diverted to the tip-tilt sensors. This will induce almost no loss on the science beams, the fringe sensors working in the H- and K-bands. The demonstrator will use VLTI near-IR tip-tilt sensor at a very low closed loop frequency. Indeed, at 2.2 μm on the siderostats, the atmospheric tip-tilt does not need to be compensated (or will be compensated well enough by the siderostat star tracker), and only the slow field rotation motion has to be measured and compensated for.

The tip-tilt mirrors will have a range equivalent to 30" on the sky and a resolution of 0.05" on the sky.

4.4. Beam compressor and differential delay lines

The beam compressors (80 to 18 mm) and differential delay lines (DDL) developed for the VLTI and for PRIMA facility will here be used. Their performance specifications are fully compliant with the demonstrator requirements. The DDL are even over-dimensioned. Indeed, the demonstrator will use baselines up to 50 m, to limit the effects of longitudinal atmospheric dispersion, leading to ± 7 mm DDL optical path strokes, well below the 60 mm maximum path stroke of DDL.

4.5. Fringe sensor unit

The demonstrator will need ideally 2 fringe trackers / fringe sensors. One could be enough if high speed (100 Hz) beam switching can be implemented on it, by means of *e.g.* polarization modulators. The demonstrator will use the fringe sensor unit (FSU) and astrometric camera developed for PRIMA. Their high sensitivity (co-phasing possible with only 1000 star photons per ms in the laboratory) and high accuracy (30 nm RMS OPD residuals in co-phasing mode) make them particularly suited for the demonstrator, leading to quite high limiting magnitudes (see sect. 4.7) for siderostats. The PRIMA FSUs will probably implement an ABCD discrete phase modulation co-axial concept, using achromatic phase-shifts which are polarization dependent. So care has to be paid to the polarization states of the demonstrator interfering beams. The fringe detection will be made in H- and K-bands. Group delay measurements in both bands will allow to get rid of the longitudinal atmospheric dispersion and to perform accurate group delay tracking.[19]

Spatial filtering via optical fiber will be done in the FSU, and adapted to the useful part of the beam size in the lab ($\leq$18 mm). With the magnification factor of the siderostat setup, this corresponds to an on sky diffraction pattern of at least 1.4" (FWHM) in the K-band. The smallest angular separation between two stars may be twice this value, but this topic has to be further investigated with the FSU design and fringe measurement.

The fringe sensor units will be closely interfaced with metrology injection optics in order to have as few non-common paths as possible. The demonstrator metrology will have to use these injection optics.

4.6. Differential metrology

The differential metrology will be the key of the demonstrator. It will have two roles : verify that the pupil is correctly transferred by the VCM, and determine the differential delay between the two paths along each interferometer arm.

Its principle will be based on a telescope-wise or arm-wise scheme, with injection of the metrology as close to the star beam combination as possible, through the central obscuration, making the input metrology pupil coincide with the star end pupil in the interferometric laboratory. The metrology beams will be propagating backward along the star optical paths. They will be polarized similarly to the star light in order to be correctly re-directed at the beamsplitter level. In the delay lines, the metrology beams will continue to propagate backward, in the central obscuration of each star beam. The pupils of both beams being transferred on the 45° mirror in the siderostats, multi-axial fringes will there be observed. Their orientation and inter-fringe will depend on the angle between the two stars, while their phase will be proportional to the optical path difference of the two metrology beams. The path length difference of the two star-light beams will be estimated for each arm, with adequate correction for longitudinal air dispersion.

As the metrology will work telescope-wise and as detection will be made at the siderostat level, a single laser source can be used for both interferometer arms. It must be single-mode, which is easy to get using single-mode injection fibers. Its frequency stability is given by the relative uncertainty required on differential path measurement, say a few 10^{-7}, or a few nm for 0.01 m differential path. A CCD camera being used for the measurement of the metrology fringe pattern at the siderostat, the laser source can be a 780 nm frequency-stabilized laser diode. The output power, continuously adjustable up to several milli-Watts, will be large enough for fringe measurement at the camera refreshing rate.

The number of metrology fringes at M4 is proportional to the angle between the two light paths in the interferometer arm. With an angle ranging from 15 to 150" (or 3 to 30" on sky), the number of fringes will be in the range 2 to 20, with a 2 cm metrology beam cross-section. With 256x256 pixels for the metrology CCD camera, the fringe pattern will be oversampled so that measurements with a few phase degrees uncertainty should be possible, the Signal/Noise ratio being then large enough.

4.7. Sensitivity and resolution

The sensitivity of the demonstrator will be limited by two devices : the star trackers at the siderostat level on a visible star, and the fringe tracker in the interferometric laboratory on the near-IR star. The visible and near-IR stars will not be necessarily the same. Provided their angular distance be smaller than 13'(star tracker field of view), the siderostat will be able to track off-axis while maintaining the target stars on-axis.

The tracking CCD camera will be an ESO technical CCD with a quantum efficiency of 50 % , pixels of 22 μm and a read-out noise of 30 e^- RMS. To get a centroïding accuracy of 0.15" (a tenth of the spot size), a signal-to-noise ratio of 10 will be required. This leads to a limiting tracking magnitude $V = 9$.

The fringe trackers will need 1000 photons per ms, in the interferometric laboratory to co-phase the telescope with a 30 nm residual error. But such a high sensitivity in fringe tracking will not be required. The fringe tracker should be able to perform coherencing with only 50 photons per ms. Taking into account all reflections and the 50 % loss at the beamsplitter, this leads to a limiting magnitude of $K = 7.5$ for the *bright* targets.

On long integration times, the uncertainty on residual delay measurements should be smaller than 5 nm (specifications for PRIMA), while differential metrology uncertainty should show about the same figure. If the ultimate accuracy in differential astrometry were limited by this simplified metrology setup, improvements could be obtained with the high resolution metrology being studied for PRIMA. Then the demonstrator performances will probably be limited by the off-axis optical quality of the VCM and other optical errors. On the other hand, residual atmospheric jitter is about 6 nm (RMS value) for 30 mn integration and 10" angular distance, so that the astrometric uncertainty should reach 25 μas with a 50 m baseline.

5. CONCLUSION

In this paper, we have associated or linked together wide-angle and narrow-angle astrometry in long-baseline optical interferometry. By analogy with a two-stage rocket, in which an heavy first-stage is supporting a much lighter second-stage, we can say that a single-field or wide-angle astrometric facility should form the robust support of the much finer task of dual-field astrometry. The first one relies mainly on stability of the interferometer arms, on accurate measurements of long optical paths and on overall reliability of baseline calibration. The second one relies mainly on very sensitive differential metrology and residual phase measurements, and most importantly on a unique baseline effectively realized for the two "interferometers in parallel".

The first VLTI equipments at Paranal (test siderostats, main delay lines and transfer optics) are expected to fulfill the requirements for an astrometric demonstration experiment, although not intended for in their initial design: the opto-mechanical parts, from the siderostat inputs to the interferometric laboratory are at a top quality, and pupil transfer along the interferometer arms, through the cat's eye of the main delay lines and their VCM, is the most adequate for stiffening the optical paths. Furthermore, the field of view of each interferometer arm is large enough for the dual-field separator to be housed in the lab. An astrometric demonstration experiment can then be conducted with these equipments.

The preliminary proposal for an astrometric demonstrator with the test siderostats has evolved in order to use as much as possible several parts being studied for the PRIMA facility: Fringe Sensor Unit, Differential Delay Lines, and possibly differential metrology. With an improved mastering of the VLTI equipments for astrometric observations at Paranal, significant scientific returns should be obtained one or two years earlier than previously expected, most of the control software for the astrometric modes of PRIMA being tested and debugged in advance with the demonstrator.

REFERENCES

1. M. Colavita, M. Shao, B. Hines, J. Wallace, Y. Gursel, F. Malbet, J. Yu, H. Singh, and C. Beichman, "ASEPS-0 testbed interferometer," in *Amplitude and Intensity Spatial Interferometry II*, J. Breckinridge, ed., *Proc. SPIE* **2200**, pp. 89–97, 1994.
2. M. Colavita, J. Wallace, B. Hines, Y. Gursel, F. Malbet, D. Palmer, X. Pan, M. Shao, J. Yu, A. Boden, P. Dumont, J. Gubler, C. Koresko, S. Kulkarni, B. Lane, D. Mobley, and G. van Belle, "The Palomar Testbed Interferometer," *Astrophys. J.* **510**, pp. 505–521, 1999.
3. M. Shao and M. Colavita, "Potential of long-baseline infrared interferometry for narrow-angle astrometry," *Astron. Astrophys.* **262**, pp. 353–358, 1992.
4. O. von der Lühe, D. Ferrand, B. Koehler, N. Zhu, and T. Reinheimer, "The interferometric mode of the ESO Very Large Telescope," in *Amplitude and Intensity Spatial Interferometry II*, J. Breckinridge, ed., *Proc. SPIE* **2200**, pp. 168–179, 1994.
5. J.-M. Mariotti, C. Denise, F. Derie, M. Ferrari, A. Glindemann, B. Koehler, S. Lévêque, F. Paresce, M. Schöller, M. Tarenghi, and M. Verola, "The VLTI program: a status report," in *Astronomical Interferometry*, *Proc. SPIE* **3350**, pp. 800–806, 1998.
6. A. Glindemann, R. Abuter, F. Carbognani, F. Delplancke, F. Derie, A. Gennai, P. Gitton, P. Kervella, B. Koelher, S. Lévêque, G. de Marchi, S. Menardi, A. Michel, F. Paresce, T. Phan-Duc, M. Schöller, M. Tarenghi, and R. Wilhem, "The VLTI-the Observatory of the 21st Century," *ESO Messenger* **98**, pp. 2–7, 1999.

7. A. Quirrenbach, V. C. du Foresto, G. Daigne, K.-H. Hofmann, R. Hofmann, M. Lattanzi, R. Osterbart, R. le Poole, D. Queloz, and F. Vakili, "PRIMA-study for a dual-beam instrument for the VLT Interferometer," in *Astronomical Interferometry, Proc. SPIE* **3350**, pp. 807–817, 1998.
8. G. Daigne, P. Dierich, and J.-F. Lestrade, "Démonstrateur astrométrique en interférométrie double-champ: une proposition pour le Paranal," in *Atelier GAIA*, M. Froeschlé and F. Mignard, eds., pp. 189–194, Observatoire de la Côte d'Azur, France, 1999.
9. F. Derie, E. Brunetto, and M. Ferrari, "The VLTI test siderostats are ready for first light," *ESO Messenger* **97**, pp. 12–14, 1999.
10. M. Shao, "Astrometry with optical/IR interferometers," in *Science with the VLT Interferometer*, F. Paresce, ed., pp. 48–54, Springer-Verlag, 1997.
11. M. Shao, M. Colavita, B. Hines, D. Staelin, D. Hutter, K. Johnston, D. Mozurkewich, R. Simon, J. Hershey, J. Hughes, and G. Kaplan, "The Mark III stellar interferometer," *Astron. Astrophys.* **193**, pp. 357–371, 1988.
12. D. Mozurkewich, D. Hutter, K. Johnston, R. Simon, M. Shao, M. Colavita, D. Staelin, B. Hines, J. Hershey, J. Hughes, and G. Kaplan, "Preliminary measurements of star positions with the Mark III stellar interferometer," *Astron. J.* **95**, pp. 1269–1277, 1988.
13. C. Hummel, D. Mozurkewich, N. Elias, A. Quirrenbach, D. Buscher, J. Armstrong, K. Johnston, R. Simon, and D. Hutter, "Four years of astrometric measurements with the Mark III optical interferometer," *Astron. J.* **108**, pp. 326–336, 1994.
14. L. Lindegren, S. Röser, H. Schrijver, M. Lattanzi, F. van Leeuwen, M. Perryman, P. Bernacca, J. Falin, M. Froeschlé, J. Kovalevsky, H. Lenhardt, and F. Mignard, "A comparison of ground-based stellar positions and proper motions with provisional Hipparcos results," *Astron. Astrophys.* **304**, pp. 44–51, 1995.
15. F. Mignard and M. Froeschlé, "Global and local bias in the FK5 from the Hipparcos data," *Astron. Astrophys.* **354**, pp. 732–739, 2000.
16. F. Martin, R. Conan, A. Tokovinin, A. Agabi, J. Borgnino, A. Ziad, and M. Sarazin, *Report on the GSM measurement campaign at the Paranal observatory*, U.M.R. Astrophysique, Université de Nice, 1999.
17. S. Esposito, A. Riccardi, and B. Femenia, "Differential piston angular anisoplanatism for astronomical optical interferometer," *Astron. Astrophys.* **353**, pp. L29–L32, 2000.
18. P. Lawson, J. Baldwin, P. Warner, R. Boysen, C. Haniff, J. Rogers, D. St-Jacques, D. Wilson, and J. Young, "Multi-wavelength fringe measurement with a CCD spectrometer at COAST," in *Astronomical Interferometry, Proc. SPIE* **3350**, pp. 753–761, 1998.
19. G. Daigne and J.-F. Lestrade, "Astrometric optical interferometry with non-evacuated delay lines," *Astron. Astrophys. Suppl. Ser.* **138**, pp. 355–363, 1999.
20. S. Lévêque and B. Koehler, "Calibration of systematic optical path differences for the very large telescope interferometer (VLTI)," in *Astronomical Interferometry, Proc. SPIE* **3350**, pp. 380–388, 1998.
21. M. Ferrari and F. Derie, "Variable curvature mirrors," *ESO Messenger* **97**, pp. 11–12, 1999.
22. *The Hipparcos Catalogue*, SP-1200, ESA, 1997.
23. R. Wielen, H. Schwan, C. Dettbarn, H. Lenhardt, H. Jahreiss, and R. Jaehrling, *Sixth Catalogue of Fundamental Stars (FK6), Part I: Basic fundamental stars with direct solutions*, ARI-Heidelberg Veroeffentlichungen No. 35, 1999.
24. A. Alonso, S. Arribas, and C. Martinez-Roger, "The empirical scale of temperatures of the low main sequence (F0V-K5V)," *Astron. Astrophys.* **313**, pp. 873–890, 1996.
25. C. Turon, M. Crézé, D. Egret, A. Gomez, M. Grenon, H. Jahreiss, Y. Réquième, A. Argue, A. Bec-Borsenberger, J. Dommanget, M. Mennessier, F. Arenou, M. Chareton, F. Crifo, J. Mermilliod, D. Morin, B. Nicolet, O. Nys, L. Prévot, M. Rousseau, and M. Perryman, *The Hipparcos Input Catalogue*, SP-1136, ESA, 1992.
26. J. Dommanget and O. Nys, "Catalogue of the Components of Double and Multiple systems (CCDM)-First edition, June 1994," *Bull. Inf. Centre Données Stellaires* **46**, pp. 3–, 1995.
27. T. Henry and D. McCarthy, "The mass-luminosity relation for stars of mass 1.0 to 0.08 solar mass," *Astron. J.* **106**, pp. 773–798, 1993.
28. G. Marcy, W. Cochran, and M. Mayor, "Extra-solar planets around main sequence stars," in *Protostars and Planets IV*, University of Arizona Press, Tucson, (in press), 1999.
29. J. Halbwachs, F. Arenou, M. Mayor, S. Udry, and D. Queloz, "Exploring the Brown-Dwarf desert with Hipparcos," *Astron. Astrophys.* , (in press), 2000.